

A Non-linear Strain-rate Micro-mechanical Composite Material Model for Impact Problems

Ala Tabiei^{*}, Sandeep Medikonda^{*}

^{*}Department of Mechanical and Materials Engineering, University of Cincinnati, Cincinnati, Ohio 45221, USA

Abstract

A micro-mechanical composite material model is developed to simulate the behavior of uni-directional composites under impact loading conditions in LS-DYNA[®]. The non-linear strain-rate and pressure dependency in the composite material model is accounted by the resin, which uses previously developed state-variable viscoplastic equations. These equations have been originally developed for metals, however are modified to account for the significant contributions of hydrostatic stresses typically observed in polymers. The material model also uses a continuum damage mechanics (CDM) based failure model to incorporate the progressive post-failure behavior. A set of Weibull distribution functions are used to quantify this behavior and a methodology of assigning physical significance to the choice of damage/softening parameters used in these functions is presented. The impact response of composite laminate plates has been simulated and compared to the experiments. In addition, the effect of hydrostatic stresses on impact problems has been further studied in detail. It has been observed that the predicted results compare favorably to the experiments.

Keywords: Unidirectional composites; Micro-mechanical model; Continuum damage mechanics; Impact response; Finite Element Method; LS-DYNA

1. Introduction

Predicting an accurate behavior of the laminated composite, especially for impacts which induce internal damage is a significant challenge as reported by Collombert et al. [1] and reviewed by Abrate [2], [3]. With the advancements made in computing technology, finite element (FE) simulations have become a substantial tool to study impact problems, especially with the use of an accurate material model as detailed information on the spatial and temporal distribution of damage can be made available during impact [4]. LS-DYNA has emerged as a powerful tool to carry out such analysis as it offers a fast and simple user interface to implement own complex material models.

In numerous experiments over the years, many researchers have observed that the modulus and strength of the composites increases with strain rate ([5]–[7]). This dependency of a composite response on strain rate is important in impact simulations [8]. Furthermore, many experimental works ([9]–[12]) have shown that composite sensitivity to strain rate is usually driven by the resin behavior. Hence, to accurately capture the response of a composite lamina there is a need to accurately represent the non-linear behavior of the polymer constituent.

Polymeric materials have been typically observed to exhibit non-linear behavior beyond 1-2% strain. Traditionally, this behavior was typically represented with the use of visco-elastic material models ([13], [14]). However, the use of state variable based visco-plastic material models, typically used for metals, has gained significant popularity ([15], [16]) in the last two decades. Even though the deformation response in polymers is due to the nonlinear response of long chain molecules as opposed to the propagation of dislocations for metals, a similar unified inelastic strain variable approach can still be utilized with the state variables representing a

different physical meaning. Pioneering work in developing numerical material models for polymers has been carried out by Goldberg over the years and a review of some of his earlier work can be found in [8].

In comparison to metals, polymers in general exhibit a strong pressure-dependent behavior ([17]–[19]), which results in different yielding under uniaxial tension, compression, shear and biaxial loadings. Furthermore, the assumption of volume constancy that typically holds in metals during plastification does not hold for thermoplastic polymers. This effect is particularly noticed in the tensile range (uniaxial and biaxial tensile stress states) and cannot be neglected. The reorientation of molecule chains and the presence of damages leads to anisotropic behavior of the polymers. The fore-mentioned characteristics make modelling polymers a challenge much less as a part of a micro-mechanics based composite material model. A material model that encapsulates these behaviors of polymers has been initially proposed by Goldberg [20] and further enhanced by Zheng and Binienda [21].

Capturing the failure modes accurately is another important aspect which enhances the complexity involved in the numerical modeling of composites. As observed from the work of Mayes and Hansen [22], a wide range of failure modes are to be captured for the accurate representation of a composite material model. Typically, many researchers ([4], [23], [24]) have accomplished this by using a macro-mechanical approach (where the composite material is modeled as an anisotropic, homogenous material), due to the simplicity and computational efficiency it offers. However, a more realistic and accurate way of doing this is by using micro-failure criterion (MFC) in a micro-mechanical approach (where a representative volume cell (RVC) composed of the fiber and matrix is used to represent the composite).

Typically, damage growth in polymeric composites manifests itself in the form of strain softening of the material. Matzenmiller et al. [25] developed a continuum damage mechanics (CDM) based model which utilizes the Weibull damage functions to progressively damage the material there by introducing strain softening into the constitutive response. This model has been observed to improve the prediction of impact damage on composites significantly ([4], [26]–[29]). However, these works use ad-hoc softening parameter values in the Weibull functions to predict damage depending on the composite and the structure that is being analyzed. Thereby lacking a proper way to characterize the composite material models.

The objective of the present work is to develop and enhance on the three-dimensional material model built by Tabiei and Babu [29] for predicting the impact response of unidirectional composites. As explained in the following sections, this is achieved by:

- Implementing strain-rate sensitive and pressure-dependent constitutive relations (modified Bodner-Partom viscoplastic state variable model [21], [30]) for the resin in a micro-mechanical based RVC which utilizes iso-strain boundary conditions.
- Implementing a CDM based progressive post-failure model and develop a methodology that assigns physical significance to the choice of damage/softening parameters.

2. Micro-mechanics of the uni-directional composite (UDC)

The representative volume cell (RVC) used to develop the micro-mechanical relations is shown in Figure 1. This RVC is the same as the one originally proposed by Pecknold and Rahman [31] and further used in various micro-mechanical models by Tabiei et al. in [28], [29], [32] and Medikonda et al. [33], [34]. However, for completeness a brief description of the RVC is provided here. The fibers are assumed to be of square cross-section for computational efficiency, this is especially beneficial since a model implemented in an explicit FE code uses very small-time steps to satisfy the stability criterion. The unit cell is divided into three sub-cells: one fiber sub-cell, denoted as f , and two matrix sub-cells, denoted as M_A and M_B respectively. The three sub-cells are grouped into two parts: material part **A** consists of the fiber sub-cell f and the matrix sub-cell M_A , and material part **B** consists of the remaining matrix M_B . The dimensions of the unit cell are 1×1 unit square. The dimensions of the fiber and matrix sub-cells are denoted by W_f and W_m respectively as shown in Figure 1 and defined as shown below:

$$W_f = \sqrt{V_f} ; \quad W_m = 1 - W_f \quad \dots (1)$$

Where, V_f is the fiber volume fraction. Effective stresses in the RVC are determined from the sub-cell values in two phases: first, stresses in fiber f and matrix M_A are combined to obtain effective stresses in part **A** which are then combined with stresses in matrix M_B to obtain the effective RVC stresses.

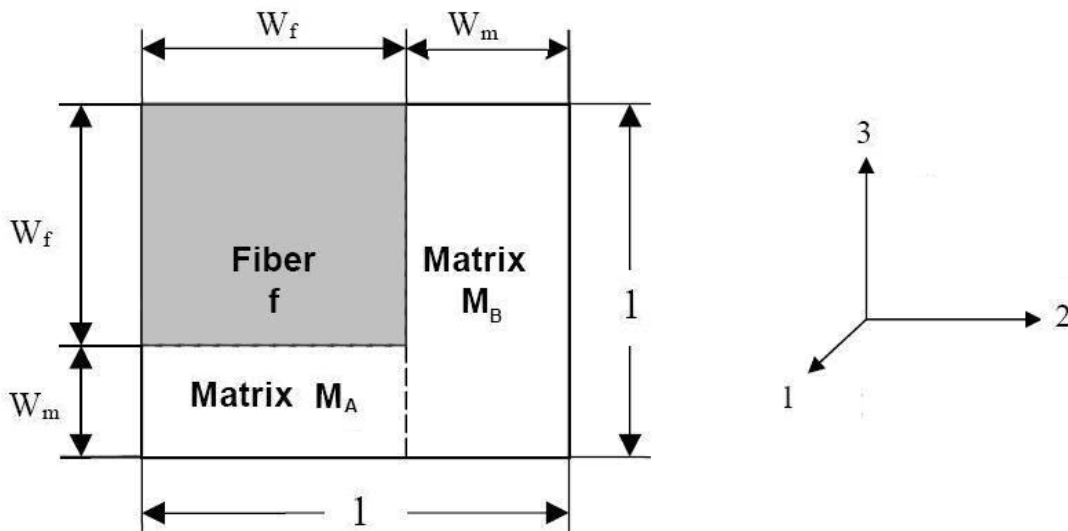


Figure 1: A representative volume cell of unidirectional fiber reinforced polymer composite

Strain-rate dependency is incorporated in the current model by using the viscoplastic relationship developed by Goldberg et al. [20] and further enhanced by Zheng et al. [21]. It should be noted that the model proposed by Goldberg et al. in [20] is a modified form of the Bodner-Partom viscoplastic state variable model, originally developed for metals. For completeness, the modified visco-plastic relations are discussed briefly in this section. Further details about the relations can be found in [20].

The total strain rate is assumed to be the sum of elastic and inelastic strain rates. The elastic strain rate is equal to the ratio of stress rate to Young's modulus of the material while the inelastic strain rate is a function of the deviatoric stress, S_{ij} , the second invariant of the deviatoric stress tensor J_2 and an isotropic state variable Z , representing the resistance to the molecular flow.

$$\dot{\epsilon}_{ij}^I = 2D_0 \exp \left[-\frac{1}{2} \left(\frac{Z}{\sigma_e} \right)^{2n} \right] \left(\frac{S_{ij}}{2\sqrt{J_2}} + \alpha \delta_{ij} \right) \quad \dots (2)$$

Where, D_0 and n are the material constants representing maximum inelastic strain rate and the rate dependence of the deformation response respectively. The effective stress σ_e , is defined as:

$$\sigma_e = \sqrt{3J_2} + \sqrt{3}\alpha\sigma_{kk} \quad \dots (3)$$

Where, α is the state variable controlling the level of hydrostatic stress effects and the 2 state variables (Z , α) are considered to be proportional to the effective deviatoric in-elastic strain rate $\dot{\epsilon}_e^I$.

$$\dot{Z} = q(Z_1 - Z)\dot{\epsilon}_e^I \quad \dots (4)$$

$$\dot{\alpha} = q(\alpha_1 - \alpha)\dot{\epsilon}_e^I \quad \dots (5)$$

The effective deviatoric in-elastic strain rate, $\dot{\epsilon}_e^I$, and the mean in-elastic strain rate, $\dot{\epsilon}_m^I$, are given by the following relations:

$$\dot{\epsilon}_e^I = \sqrt{\frac{2}{3}\dot{\epsilon}_{ij}^I\dot{\epsilon}_{ij}^I}; \quad \dots (6)$$

$$\dot{\epsilon}_e^I = \dot{\epsilon}_{ij}^I - \dot{\epsilon}_m^I \ \& \ \dot{\epsilon}_m^I = (\dot{\epsilon}_{11}^I + \dot{\epsilon}_{22}^I + \dot{\epsilon}_{33}^I)/3$$

It has to be noted that Z_1 and α_1 representing the maximum values of Z and α respectively are input as material constants along with their initial values Z_0 and α_0 . In addition, q is a material constant representing the “hardening” rate.

One procedure of determining the resin material constants can be found in the original work of Goldberg [20], alternatively the material constants can also be determined by fitting the constitutive model to the experimental results using an error minimization scheme such as the least-squares method.

It is well known that the elastic modulus significantly increases with increasing strain rate in polymers and subsequently in polymer matrix composites. Zheng and Binenda [21], drawing inspiration from the work of Yen [26], have proposed the use of a dynamic elastic moduli that accounts for the strain rate effect.

$$E_m = E_0 \left(1 + C \ln \frac{\dot{\epsilon}}{\dot{\epsilon}_0} \right); \text{ where,}$$

$$\dot{\epsilon} = \sqrt{\frac{2}{3}[(\dot{\epsilon}_{11} - \dot{\epsilon}_m)^2 + (\dot{\epsilon}_{22} - \dot{\epsilon}_m)^2 + (\dot{\epsilon}_{33} - \dot{\epsilon}_m)^2 + 2\dot{\epsilon}_{12}^2 + 2\dot{\epsilon}_{23}^2 + 2\dot{\epsilon}_{31}^2]} \quad \dots (7)$$

$$\dot{\epsilon}_m = (\dot{\epsilon}_{11} + \dot{\epsilon}_{22} + \dot{\epsilon}_{33})/3$$

Since there is no closed form solution for the first order differential equations shown in Equations (2) through (7), which formulate one differential equation per component, a numerical solution is obtained at each time step of the explicit FE time step. Since the current material model is being developed to study impact problems, there is a high degree of possibility that the model might encounter high strain increments. Hence, to ensure stability, a 4-step Runge-Kutta time integration has been performed as shown in Figure 2 for the resin material.

The fibers are linearly elastic materials and are initially transversely-isotropic but become orthotropic with damage evolution. Damages to the fibers are assumed to be a result of only the direct stresses and the shear stresses do not contribute here. This causes the damages to be oriented in the material directions of the fibers and act independently. The constitutive relations of the fibers can be written in matrix form as:

$$\{\sigma\}^f = [C_f] \{\varepsilon\}^f \quad \dots (8)$$

Where, $[C_f]$ is the stiffness matrix which can be partitioned into direct and shear stress stiffness matrices as follows:

$$[C_f] = [S_f]^{-1} = \begin{bmatrix} [S_{fd}]^{-1} & [0]_{3 \times 3} \\ [0]_{3 \times 3} & [S_{fs}]^{-1} \end{bmatrix} \quad \dots (9)$$

The direct stress compliance matrix, whose inverse is the direct stress stiffness matrix, should be symmetric and the following relationship should be obeyed:

$$\frac{\nu_{ij}}{E_i} = \frac{\nu_{ji}}{E_j} \quad , \quad i, j = 1,2,3 \text{ and } i \neq j \text{ (no summation)} \quad \dots (10)$$

The direct and shear stress compliance matrices in terms of the properties of the fibers are:

$$[S_{fd}] = \begin{bmatrix} \frac{1}{(1-d_1)E_1} & -\sqrt{\frac{\nu_{12}}{(1-d_1)E_1} \frac{\nu_{21}}{(1-d_2)E_2}} & -\sqrt{\frac{\nu_{12}}{(1-d_1)E_1} \frac{\nu_{21}}{(1-d_3)E_2}} \\ \frac{1}{(1-d_2)E_2} & & -\frac{\nu_{23}}{\sqrt{(1-d_2)E_2(1-d_3)E_2}} \\ \text{Symm.} & & \frac{1}{(1-d_3)E_2} \end{bmatrix} \quad \dots (11)$$

$$[S_{fs}] = \begin{bmatrix} \frac{1}{G_{12}} & 0 & 0 \\ & \frac{1}{G_{23}} & 0 \\ \text{Symm.} & & \frac{1}{G_{o12}} \end{bmatrix} \quad \dots (12)$$

Where E_1, E_2 are the longitudinal and transverse moduli of the fibers respectively, $\nu_{ij}, i, j = 1,2,3$ and $i \neq j$, are its Poisson's ratios, G_{o12}, G_{12} are its initial and strain-rate dependent in-plane shear moduli respectively, G_{23} is its transverse shear moduli, and $d_i, i = 1,2,3$, are damage parameters which are discussed in the following section on progressive failure modeling.

Additionally, damages d_z, d_{yz} and d_{zx} are introduced by the inter-laminar delamination model. This model is the same as the one implemented in LS-DYNA for MAT161. Where, delamination initiation is a consequence of the quadratic interaction between the out-of-plane stresses of a lamina and is assumed to be mainly a lamina failure.

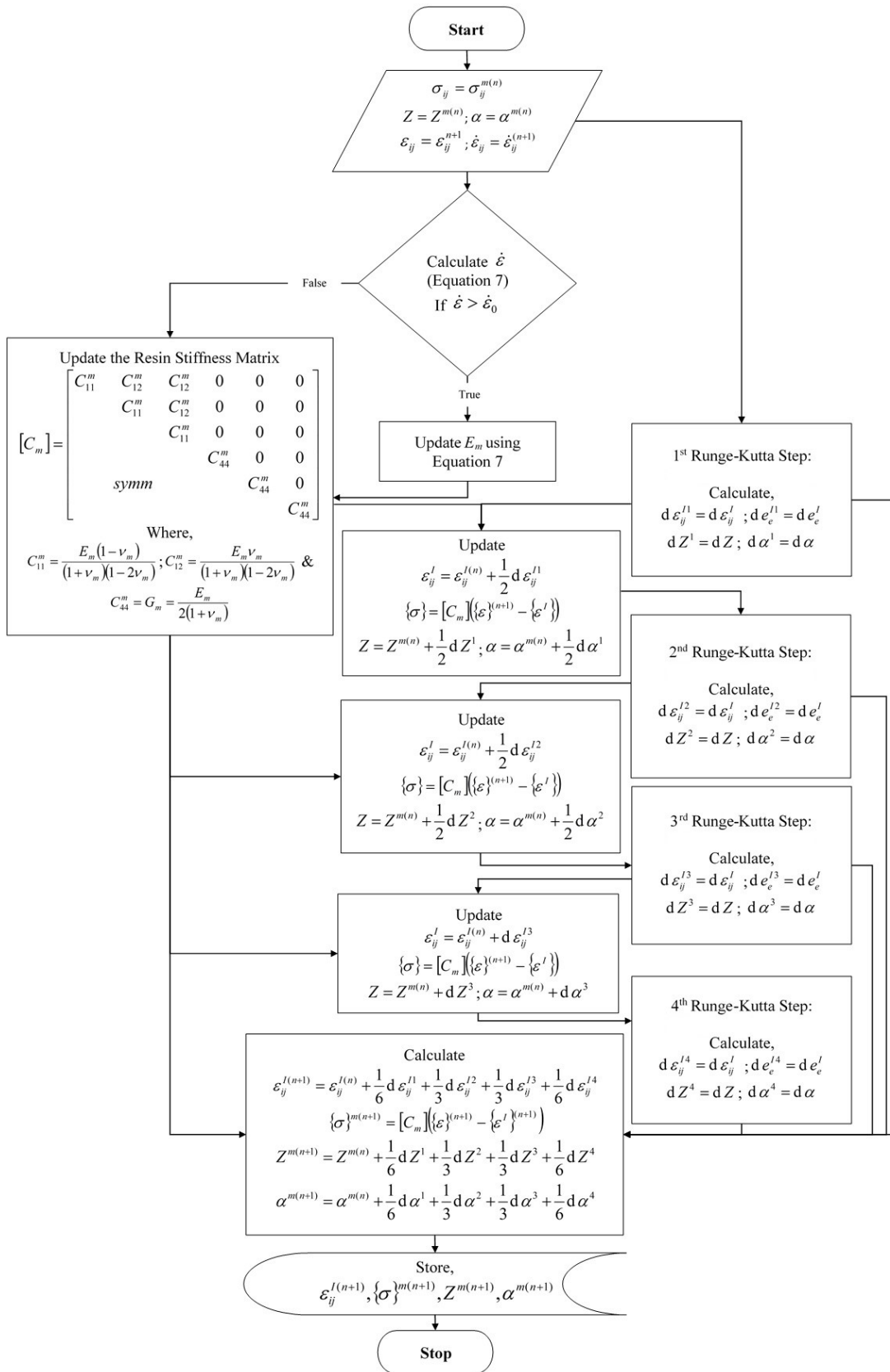


Figure 2: Illustration of a 4-step Runge-Kutta method implemented for the resin material

The loading criterion for this failure mode has the following form:

$$S^2 \left\{ \left(\frac{E_3 \langle \varepsilon_{33} \rangle}{S_{3f}} \right)^2 + \left(\frac{G_{23} \gamma_{23}}{S_{230} + S_{SR}} \right)^2 + \left(\frac{G_{31} \gamma_{31}}{S_{310} + S_{SR}} \right)^2 \right\} - r^2 = 0 \quad \dots (13)$$

It has to be noted here that the elastic material parameters specified in Equation (13) correspond to the macro-properties of the lamina, which are back calculated from the stiffness matrix assembled for the RVC as discussed by Qu and Cherkaoui [35].

The presence of friction is accounted using the Coulomb-Mohr theory via the variable S_{SR} .

$$S_{SR} = E_3 \tan \varphi \langle -\varepsilon_z \rangle \quad \dots (14)$$

Where, φ is the Coulomb's friction angle. The normal tensile and the out-of-plane shear moduli of the lamina is computed at the first time step and stored as a material property.

$d_{lam}^{(n+1)}$ is the damage variable associated with this failure mode at the current time step (denoted by the superscript $(n+1)$) and its evolution is given by the relation:

$$d_{lam}^{(n+1)} = \max \left\{ 1 - \exp \left[\frac{1}{m_d} (1 - r^{m_d}) \right], d_{lam}^n \right\} \quad \dots (15)$$

Where, r is the damage threshold as given in Equation (13) and m_d is the damage exponent for delamination. Note that $d_{lam}^{(n+1)} = d_z^{(n+1)} = d_{yz}^{(n+1)} = d_{zx}^{(n+1)}$ and $d_z^{(n+1)}$ vanishes in a compressive mode i.e., when $\varepsilon_{33} < 0$. Delamination damage is constrained at 0.10 to avoid numerical difficulties and when this maximum value is reached in an element, it is considered to be fully delaminated.

Once the stresses in all the constituent sub-cells have been obtained, they are then combined using the iso-strain boundary conditions to obtain the effective stresses of the RVC [34].

$$\sigma_{11}^{RVC} = W_f^2 \sigma_{11}^f + (1 - W_f^2) \sigma_{11}^R \quad \dots (16)$$

$$\sigma_{22}^{RVC} = W_f^2 \sigma_{22}^f + (1 - W_f^2) \sigma_{22}^R \quad \dots (17)$$

$$\sigma_{33}^{RVC} = d_z \left[W_f^2 \sigma_{33}^f + (1 - W_f^2) \sigma_{33}^R \right] \quad \dots (18)$$

$$\sigma_{12}^{RVC} = W_f V_{s4} \sigma_{12}^f + (1 - W_f V_{s4}) (1 - d_4) \sigma_{12}^R \quad \dots (19)$$

$$\sigma_{23}^{RVC} = d_{yz} \left[W_f V_{s5} \sigma_{23}^f + (1 - W_f V_{s5}) (1 - d_5) \sigma_{23}^R \right] \quad \dots (20)$$

$$\sigma_{31}^{RVC} = d_{zx} \left[W_f V_{s4} \sigma_{31}^f + (1 - W_f V_{s4}) (1 - d_6) \sigma_{31}^R \right] \quad \dots (21)$$

Since, the use of iso-strain boundary conditions for shear isn't quite realistic in a physical sense [33], different ad-hoc shear volume fraction coefficients, V_{s4} and V_{s5} , for the in-plane and transverse shear have been introduced and have values quite lower than the volume fraction of the fibers. Damage parameters d_i , $i = 4, 5, 6$, represent the damages imposed on the matrix material and affect only the shear stresses of the resin. They will be further discussed in the next section.

3. Damage evolution and characterization

Damage is considered an irreversible process and has been implemented as such in the current model preserving the thermodynamic constraints of damage mechanics. In their work, Matzenmiller et al. [25] proposed an approach which used a Weibull distribution function to describe the damage evolution as a function of strain over the entire load range. Depending on the failure mode considered, a slightly modified version of this model is used here. Fibers are assumed to govern the behavior of the composite in direct loading, while the matrix is assumed to dictate the response in the shear directions.

$$d_k^{(n+1)} = \max \left\{ 1 - \exp \left[- \frac{1}{m_k} e \left(\frac{\sigma_{ij \ t|c}^{fud}}{\sigma_{k \ t|c}} \right)^{m_{fk}} \right], d_k^{(n)} \right\} \quad \dots (22)$$

where, $ij = 12, 23$ or 31 and $k = 1, 2$ or 3

$$d_k^{(n+1)} = \max \left\{ 1 - \exp \left[- \left(\frac{|\mathcal{E}_{ij}|}{\mathcal{E}_{km}} \right)^{m_s} \right], d_k^{(n)} \right\} \quad \dots (23)$$

where, $ij = 12, 23$ or 31 and $k = 4, 5$ or 6

Where, $t|c$ denotes tension or compression. When a positive strain is detected, the parameters for tension are utilized otherwise the parameters provided for compression are used. $\sigma_{ij \ t|c}^{fud}$ is the undamaged stress in the fibers and when the damage d_1 reaches 0.01 in tension, the finite element is considered to be totally failed.

The damages of the matrix material on the other hand are constrained to not exceed 0.20. The primary reason for constraining the damages is to account for the numerical instabilities that arise when stress in an element goes to zero. These damages are applied on the matrix material shear stresses when the stress response of the sub-cells is calculated. It should be noted that damages for the matrix material are being applied on the stresses unlike what was done for the fibers, where the elastic moduli are reduced. The reason for this is considered to be two fold, one is because the matrix material model is assumed to be isotropic while the damages in the material are not and secondly the visco-plastic material model calculates the actual stresses of the material and not the effective stresses of the damaged material [29], [36].

The damage parameter that has been used in the Weibull functions above has been observed to be very problem dependent and difficult to characterize. A small value of the damage exponent (for ex. m_f in Equation (22)) makes the material behave in a very ductile manner and the behavior becomes increasingly brittle as this value increases. Hence, it is difficult to obtain the softening response of most quasi-brittle materials. The softening response heavily depends on the set-up and test machines, which can lead to very different results. The choice of damage parameters for each mode has been debated by Vaziri et al. [4] and Tabiei et al. [29]. A procedure for the calculation of softening parameter used in the damage evolution function has been presented in the current study.

In order to avoid undesirable localization, Bazant and Oh [37] proposed the crack band theory. According to this theory, regardless of the choice of mesh, the overall energy dissipation due to damage must remain constant. This concept was further used by Pinho [38] and subsequently Cousigne [39], who have discussed a smeared formulation involving damage variables, where a length parameter has been introduced into the damage constitutive law. Their work primarily relies on the calculation of failure strain based on the fracture toughness, which is subsequently used to calculate the damage in the composite. This calculation of a failure strain is of little consequence to the damage function discussed in the current work. Hence, a numerical algorithm which iteratively solves for the softening parameter has been presented.

The total energy absorbed by one element after failure can be expressed by:

$$U = V * U_{vol} \quad \dots (24)$$

Where, U_{vol} is the total energy absorbed per unit volume, in simpler terms it is area captured under the stress-strain curve before and after the onset of failure. The volume of the element is denoted by V . Based on Figure 3, the total energy can also be represented in terms of the fracture plane area A and the energy per unit area or the fracture toughness Γ .

$$U = A * \Gamma \quad \dots (25)$$

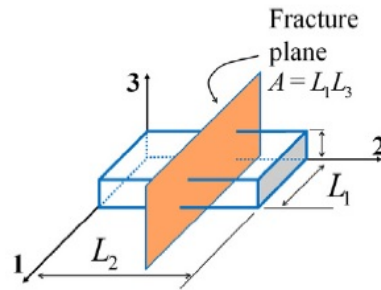


Figure 3: Fracture plane for a load [39]

Equations (24) and (25) can be equated and the energy dissipated per unit volume absorbed by an element is given by the following relation:

$$U_{vol} = \Gamma * \frac{A}{V} = \frac{\Gamma}{l} \quad \dots (26)$$

Where, l is the characteristic element length. For square elements, it is expressed in terms of the area at the integration point by the following relation [39]:

$$l = 1.12 * \sqrt{A_{ip}} \quad \dots (27)$$

Since, the fracture toughness Γ is a constant known value for a certain material, we can solve for the softening parameter m_f numerically as U_{vol} is known for a fixed mesh size. The procedure of accomplishing this is presented in the flowchart shown in Figure 4 and has been implemented as a user-subroutine in the material which is called at the start of any simulation.

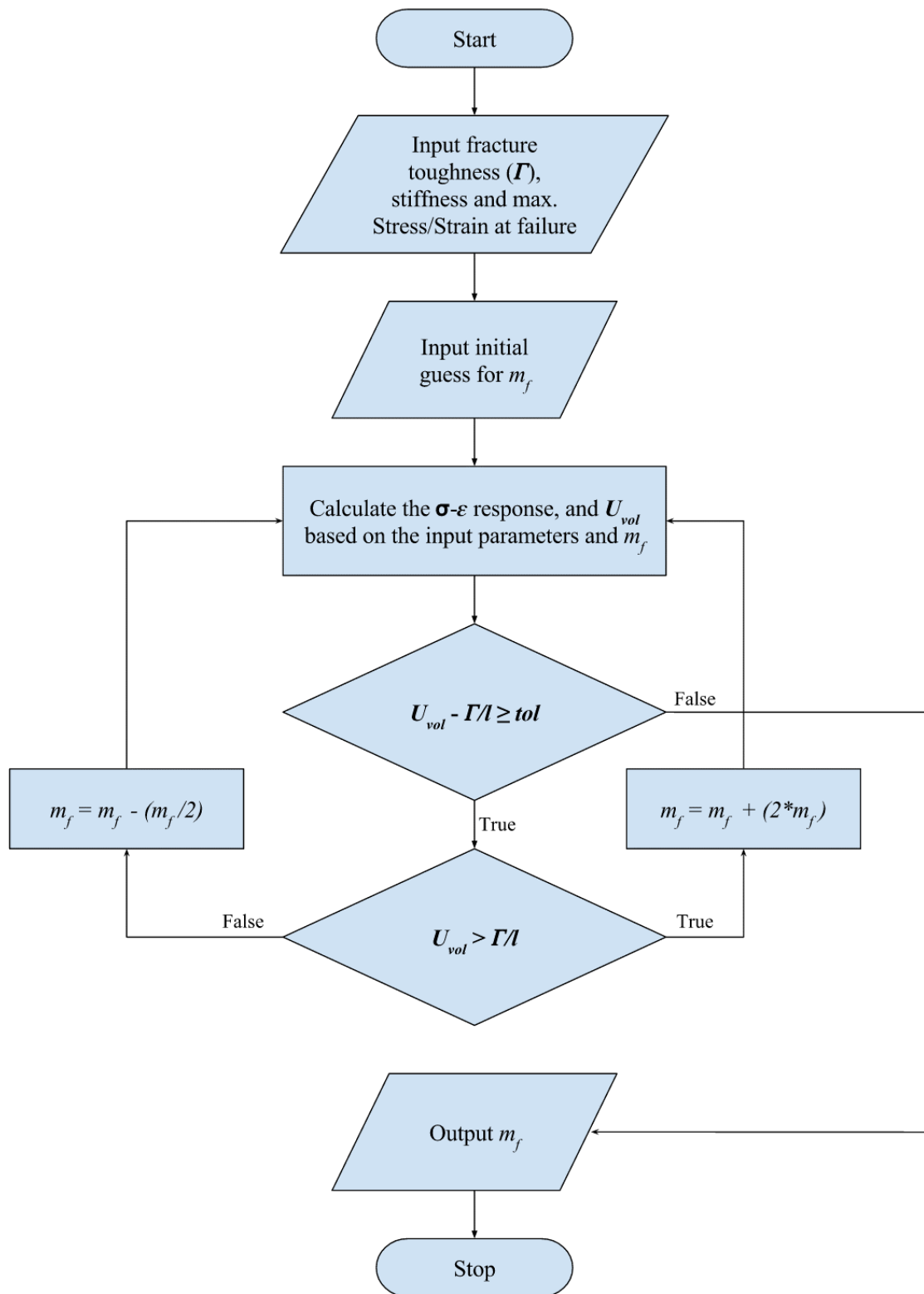


Figure 4: Flowchart demonstrating the calculation of the damage parameters

It should be noted that once the softening parameter m_f has been calculated for a certain U_{vol} and mesh size, it becomes the default value. For a new mesh/element size, U_{vol} is scaled appropriately depending on the element's characteristic length and the softening parameter is recalculated using the subroutine discussed above.

$$U_{vol}^{new} = U_{vol}^{def} * \frac{l^{def}}{l^{new}} \quad \dots (28)$$

The damage exponent is calculated individually for each element inside the mesh and this can be quite taxing for large scale problems. As it can be observed in the flowchart presented in Figure 4, the algorithm draws inspiration from the bisection method and thus determines the damage parameter rather quickly. The speed at which the damage parameter is determined is further illustrated in Figure 5, for an input/target fracture toughness of 21.7 Mpa.mm and an initial guess of 2 for the damage exponent. The solution converges in just 9 iterations. Of course, it should be noted that the speed of the solution is slightly influenced by the initial guess provided to the subroutine.

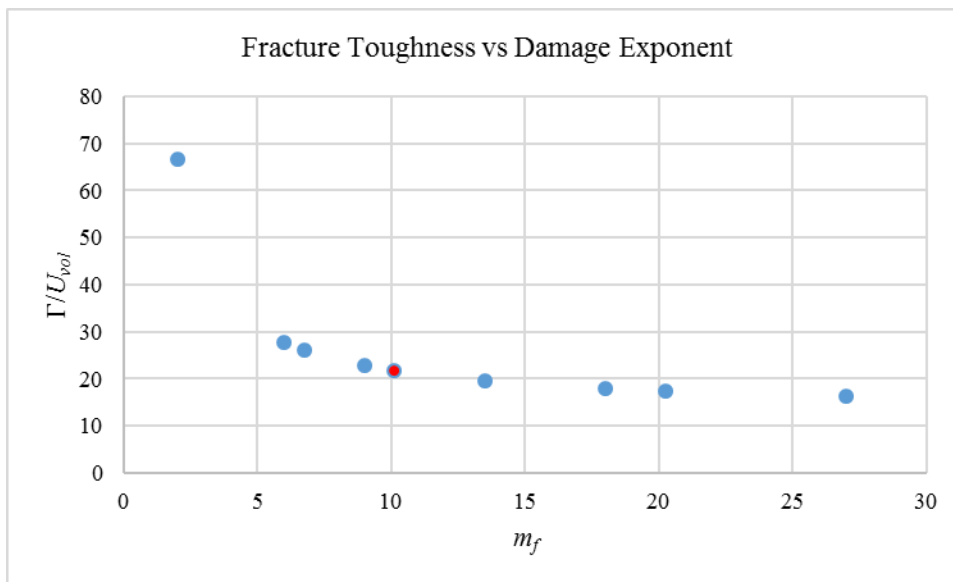


Figure 5: Fracture toughness vs Damage exponent for an element with characteristic length = 1

4. Results and Discussion

4.1 Impact on a 10-ply E-Glass/Epoxy laminate

In the current section, impact loading on E-Glass/Epoxy laminate plates has been simulated using the composite material model discussed so far. The experiments have been carried out in a drop-weight setup by Collombet et al. [1]. The plates are circular with a diameter 200 mm and a thickness of 1.8 mm. They are put together by stacking 10 unidirectional plies in one of the 3 configurations $[0_n / 90_m / 0_n]$, where $2n + m = 10$ with $n = 2, 3, 4$. The cylindrical projectile impacting the laminate plates with an incident energy of 27 J has a hemispherical end of mass 2.3 Kg, density 7.8 Kg/m³, length 600 mm, diameter 25 mm, and the following properties: $E = 210 \text{ GPa}$, $\nu = 0.3$. The plates are clamped on their periphery over a 20 mm wide ring and a uniform pressure is applied on the ring by means of springs. Additional details of the setup can be found in [1].

The finite element models used in the simulations are shown in Figure 6. As seen in these figures, only a quarter of the experimental setup is modeled due to symmetry, this helps reduce the computational effort. In addition, simulations are carried out for a coarse mesh (Figure 6 (a)) and a fine mesh (Figure 6 (b)). As seen in Figure 6 (c), each lamina is modeled using a single layer of solid elements. The support on which the laminate rests is completely constrained at the bottom and is modelled as a rigid material. The ring is constrained from moving in the vertical Z-direction to account for the pressure applied on it, this replicates the uniform pressure applied on the springs [1]. Lastly, the impactor is modelled as a rigid material as well and only the contact surface of the hemispherical end is modeled using shell elements. Eroding surface-to-surface contact is defined between the impactor and the plates while automatic surface-to-surface contact is defined between the support, ring and the plates. The constituent properties and parameters used in the simulations are given in Table 1. It has to be noted that, some of the required material parameters which are not available in [1] have either been obtained from the literature [8], [21], [29], [36] or valid estimates have been used. For example, the parameters required for the viscoplastic constitutive relations of the Epoxy resin are not available directly in the literature and neither are their uni-axial and shear responses at different strain-rates from which they can be determined. Hence, the parameters of the Epoxy used are based on the values provided for the E-862 resin [21] which shares similar elastic properties with the Epoxy resin.

V_f	$\dot{\epsilon}_o (s^{-1})$	$E_1(GPa)$	ν_{12}	$X_t(Mpa)$	$X_c(Mpa)$	$E_2(GPa)$	ν_{23}
0.43	1×10^{-3}	74	0.25	3500	1600	4.93	0.25
$\sigma_{2t}(Mpa)$	$\sigma_{2c}(Mpa)$	$G_{o12}(GPa)$	$G_{23}(GPa)$	a_{s4}	ϵ_{4m}	ϵ_{5m}	V_{s4}
80	255	30	1.97	0.011	0.15	0.15	0.014
V_{s5}	$a_G(GPa)$	b_t	b_c	$E_m(GPa)$	ν_m	$D_0(s^{-1})$	n
0.020	0.900	1.00	1.00	3.00	0.4	1×10^6	0.80
$Z_0(MPa)$	$Z_1(MPa)$	q	α_0	α_1	C	$S_{3t}(MPa)$	$S_{230}(MPa)$
420.0	820.0	120.0	0.15	0.06	0.0	100	86
$S_{310}(MPa)$	φ (deg.)						
64	20						

Table 1: Properties and parameters of E-glass/Epoxy materials used in verification examples

Rate sensitivity of the composite material is predominantly accounted by the resin in the proposed material model. In the parametric studies carried out by Zheng [40], it has been observed that Z_1 and α_1 have a significant effect on the strain rate. Increasing values of Z_1 and decreasing values of α_1 (in tension) tend to increase the maximum/yield stress. Parameters Z_0 and α_0 on the other hand have been observed to control the starting point of the non-linearity.

Ad-hoc volume fractions control the effect that the resin behavior has on the overall composite which in turn effects its rate-dependent behavior in shear. However, this is subjective and must be determined experimentally depending on the stress-strain responses of the composite and its constituents. In general, small changes in the ad-hoc volume fraction parameters will not have a great influence on the answer.

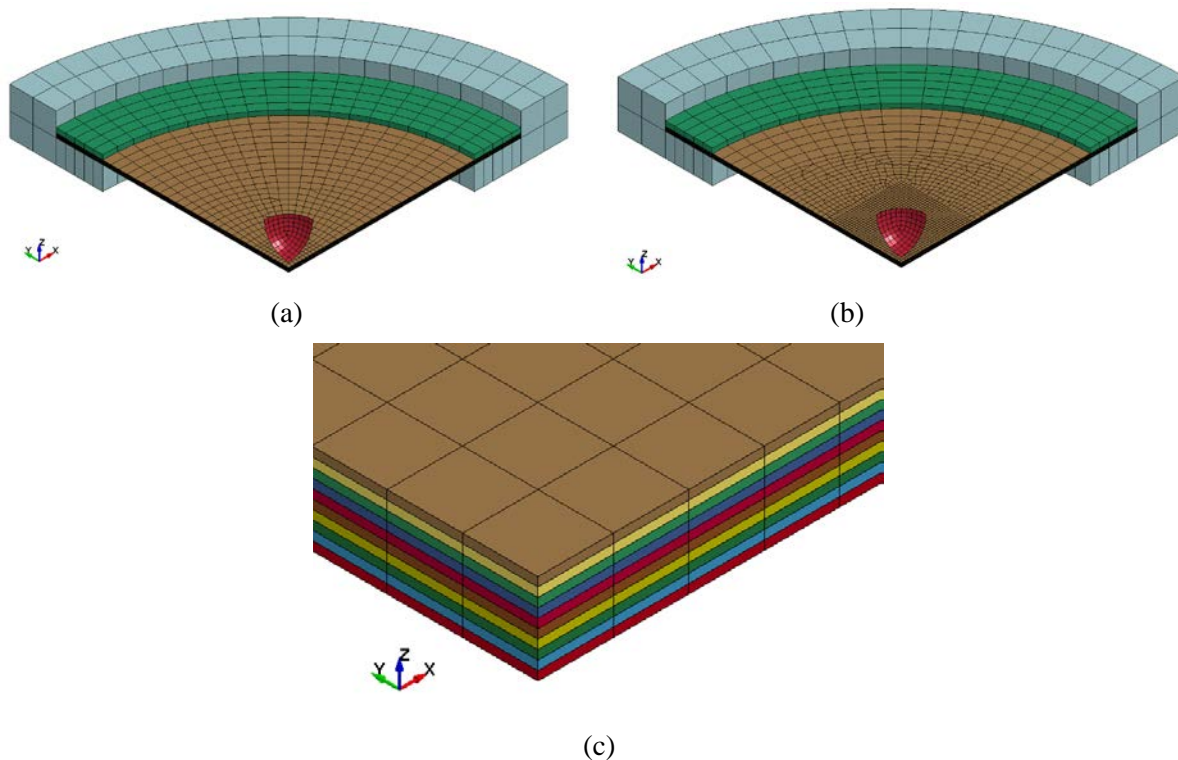


Figure 6: FE model used for FE simulation of a 27 J impact on $[0_n/90_m/0_n]$, $n = 2, 3, 4$, E-glass/Epoxy laminates – (a) full model with coarse mesh, (b) full model with fine mesh and (c) close-up view of the laminate

It is important to note that the criterion for element erosion (fiber-breakage), discussed in Section 3 has been deactivated for the cases studied. Mainly because in the experimental reference paper by Collombet et al. [1] there was no reference to any fiber breakage.

Figure 7 show the contact force vs time history for all the 3-laminates simulated along with the experimental results. It must be noted that the contact force obtained from the simulations has been multiplied by a factor of 4 since only a quarter of the model has been subjected to impact. Based on the observed results, it can be said that the effect of the mesh sizes considered has been minimum.

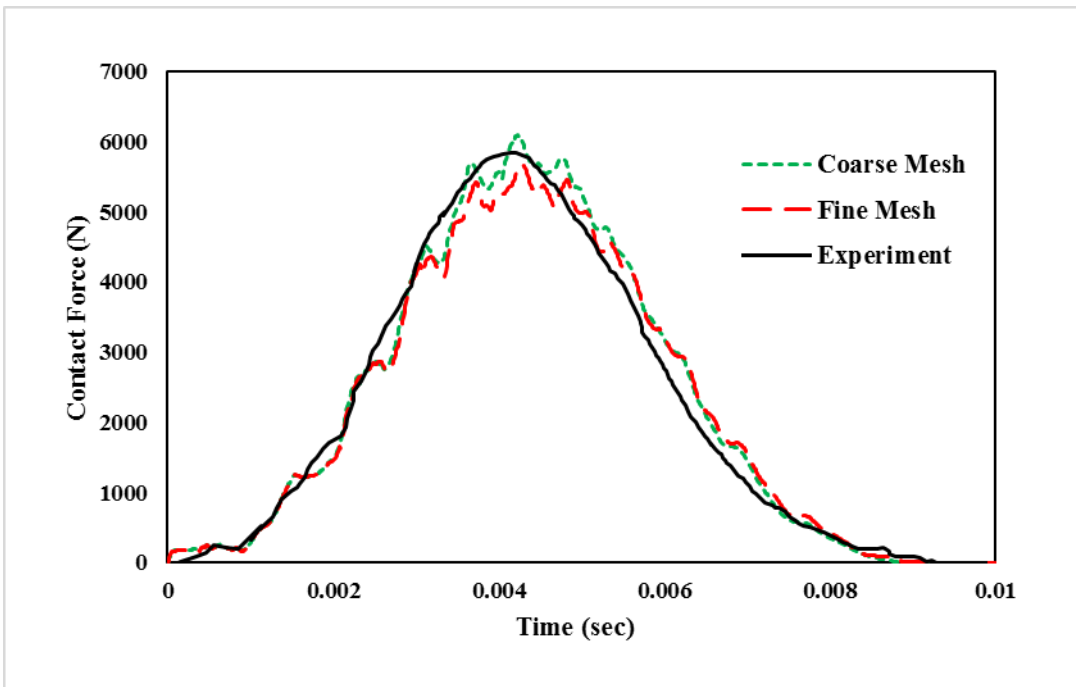


Figure 7: Contact force - time history predicted by the current model for a 27 J impact on a $[0_2/90_6/0_2]$ E-glass/Epoxy laminate

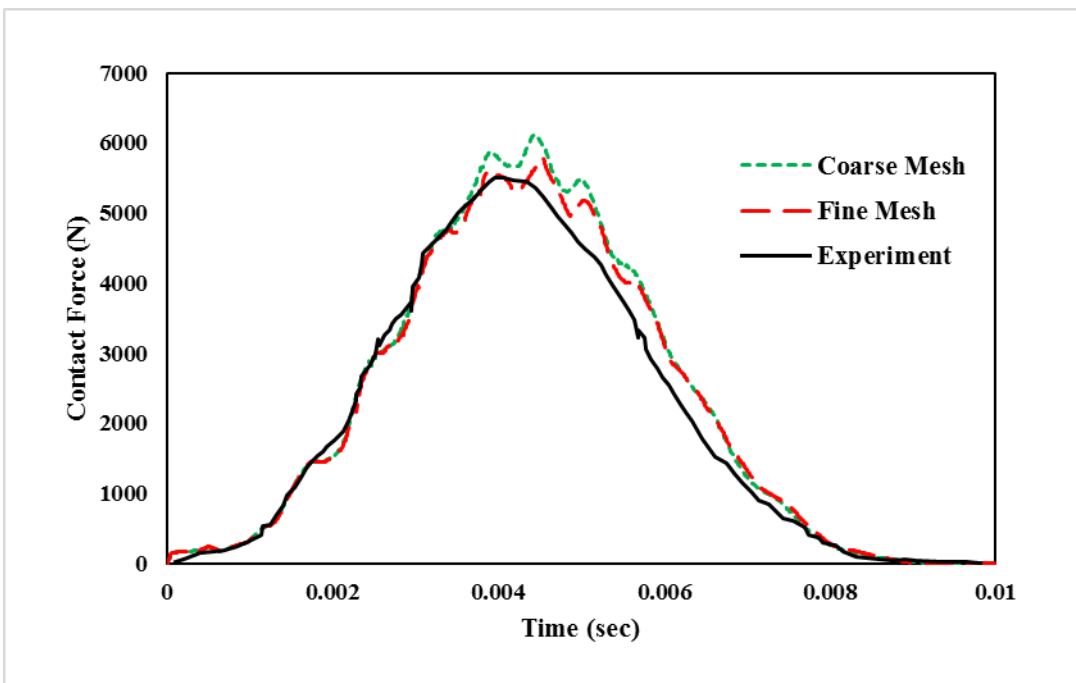


Figure 8: Contact force - time history predicted by the current model for a 27 J impact on a $[0_3/90_4/0_3]$ E-glass/Epoxy laminate

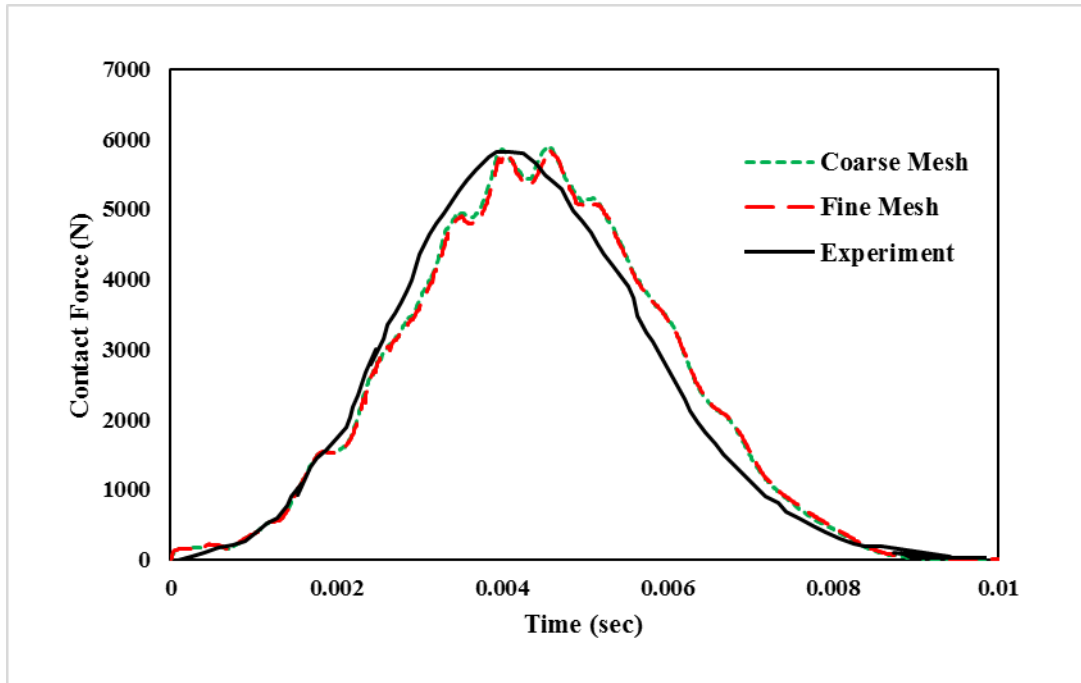


Figure 9: Contact force - time history predicted by the current model for a 27 J impact on a $[0_4/90_2/0_4]$ E-glass/Epoxy laminate

The peak contact forces obtained for the $[0_2/90_6/0_2]$ and the $[0_4/90_2/0_4]$ laminates are found to be the closest to their respective experimental results whereas the peak force predicted for the $[0_3/90_4/0_3]$ laminate is found to be slightly higher than the experimental value. However, it has to be noted that this error in peak force (which is ~5%) is still smaller than the error reported in Tabiei and Babu [29] (nearly ~7%). It must be noted that all 6 numerical simulations predict a slightly bigger mismatch during unloading possibly due to the assumed boundary conditions, contact algorithm or the approximate material properties. Overall, the predicted contact force history is found to agree reasonably well with the experimental result in each case.

4.2 Effect of Hydrostatic stresses on a 10-ply E-Glass/Epoxy laminate

As discussed in the Introduction, hydrostatic stresses have been observed to have a significant contribution to the response of a polymer. In the current model, hydrostatic stress effects are accounted through the inclusion of a state variable ' α ', this can be turned off by setting $\alpha_0 = \alpha_1 = 0.0$. In this section, the importance of having hydrostatic stresses in analyzing the impact response has been further investigated. To do this, the fine mesh models discussed in the previous section have been simulated with and without the inclusion of ' α ' and the results have been presented in Figure 10 - Figure 12.

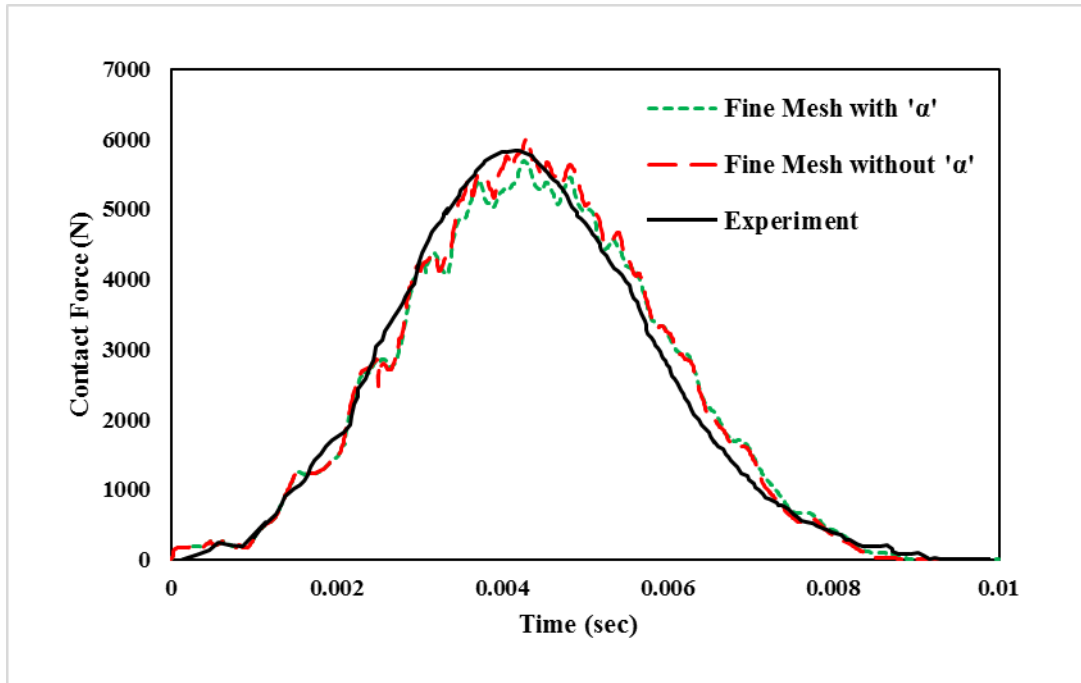


Figure 10: Contact force - time history predicted by the current model for a 27 J impact on a $[0_2/90_6/0_2]$ E-glass/Epoxy laminate with and without ' α '

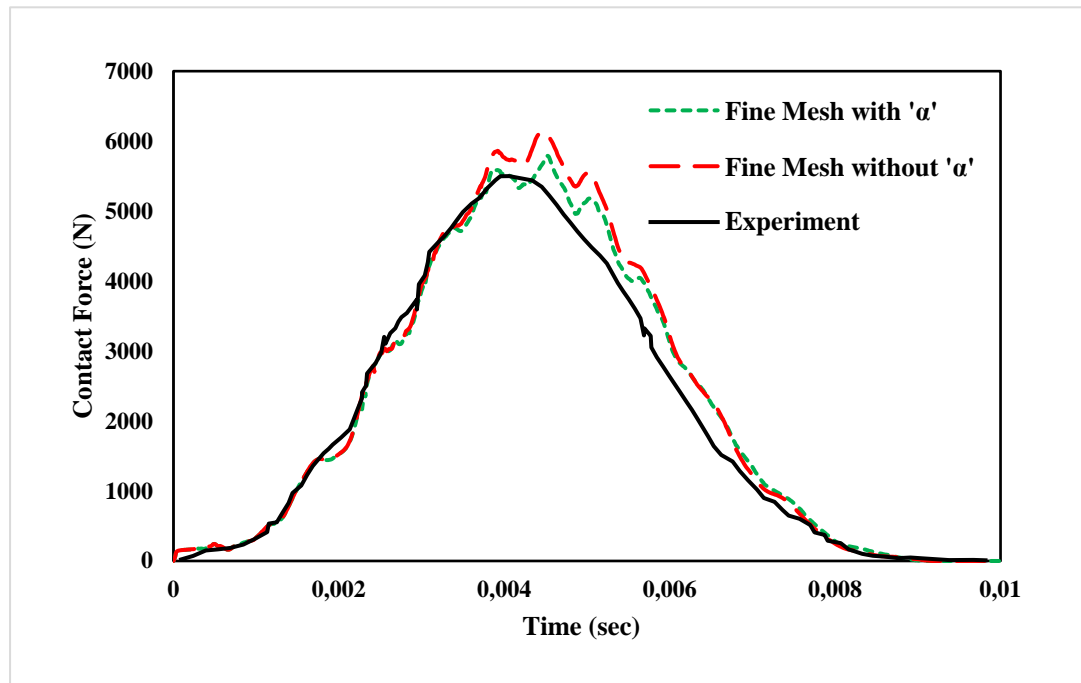


Figure 11: Contact force - time history predicted by the current model for a 27 J impact on a $[0_3/90_4/0_3]$ E-glass/Epoxy laminate with and without ' α '

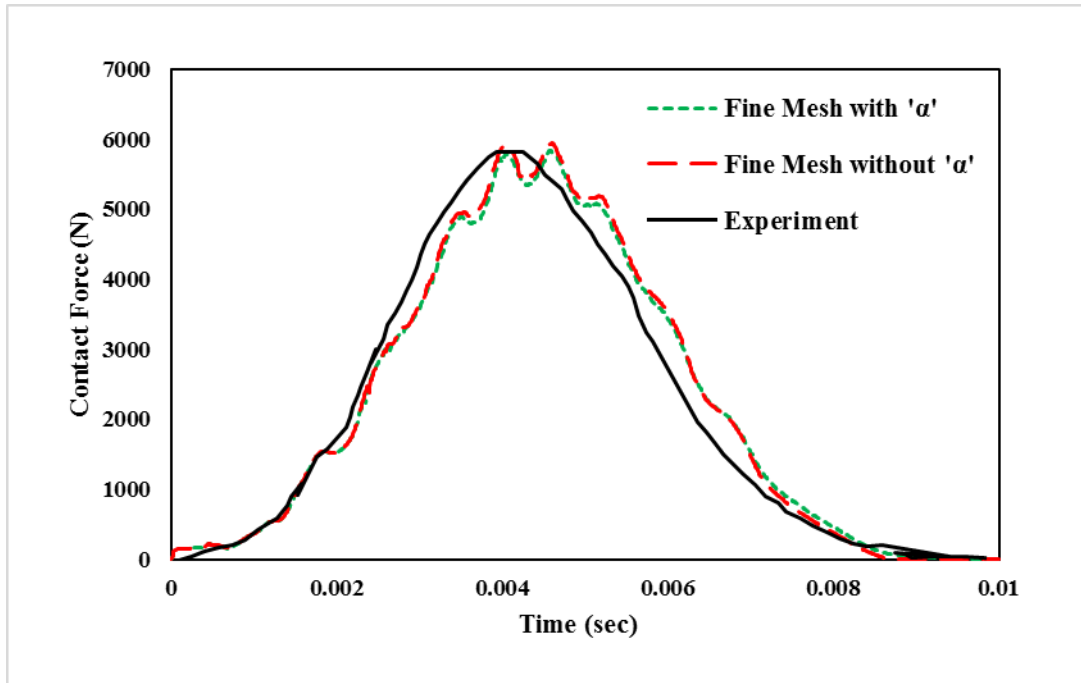


Figure 12: Contact force - time history predicted by the current model for a 27 J impact on a $[0_4/90_2/0_4]$ E-glass/Epoxy laminate with and without ' α '

Based on these results, it can be said that the peak contact force predicted by the simulations with the inclusion of hydrostatic stress effects is closer to the experimental values. The exact amount of error for each case is reported in Table 2 and the maximum error has been reported in the simulations of $[0_3/90_4/0_3]$ E-Glass/Epoxy laminate without ' α '.

Laminate Configuration	Error with experiments	
	With α	Without α
$[0_2/90_6/0_2]$	2.672%	3.178%
$[0_3/90_4/0_3]$	5.268%	11.213%
$[0_4/90_2/0_4]$	0.168%	1.992%

Table 2: Comparison of error in the peak contact force reported for each laminate configuration

4.3 Impact event on a 22-ply E-Glass/Epoxy laminate

To better understand the hydrostatic stress effects, impact events have also been carried out on a much thicker E-Glass/Epoxy plate. The finite element model used in the simulations is shown in Figure 13. Once again, to reduce the computational effort, only a quarter of the laminate is modeled due to symmetry and each lamina is modeled using a single layer of solid elements. The model consists of 22 uni-directional plies with a stacking sequence of $[45_{22}]$. The laminate modelled is square in shape with a side of length 198 mm and a thickness of 13.2 mm. Whereas, the impactor is modelled as a rigid part which has a length of 40 mm and a radius of 6.35 mm. In addition, the laminate is constrained on the top and bottom with rigid supports with a radius of 12.7 mm cut out at the corner where the impact event occurs.

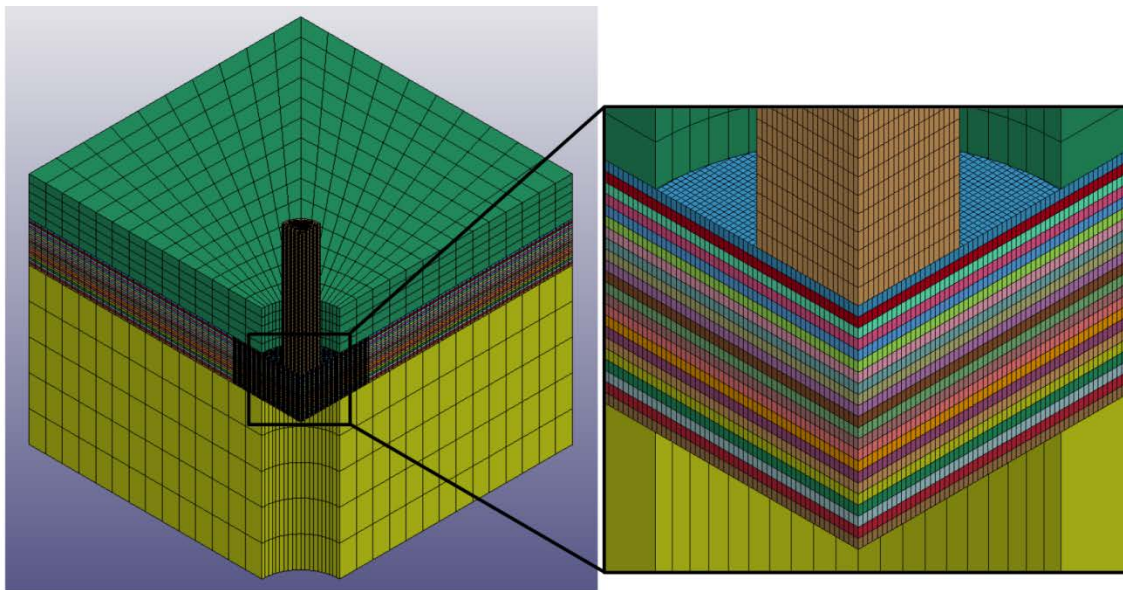


Figure 13: Full model and close-up view of the FE model used for simulation of impact on a thick plate.

Unlike the low-velocity boundary condition used in the earlier case, the impactor in the current case is being displaced by 10 mm (in the downward direction) to observe the response of the plate at a higher state of deformation. Simulations have been carried out with and without the inclusion of ' α ' to compare the effect of hydrostatic stress in predicting the contact force and the results have been presented in Figure 14. It must be noted that due to the lack of experimental data only the numerical results have been compared in this figure.

Results presented in Figure 14 show that at higher states of deformation the contribution resulting from the inclusion of ' α ' shows a significant effect on the contact force. For the current case, the simulation with ' α ' predicts a peak force of ~9,981 N, whereas the case without ' α ' predicts a value of ~8,518 N.

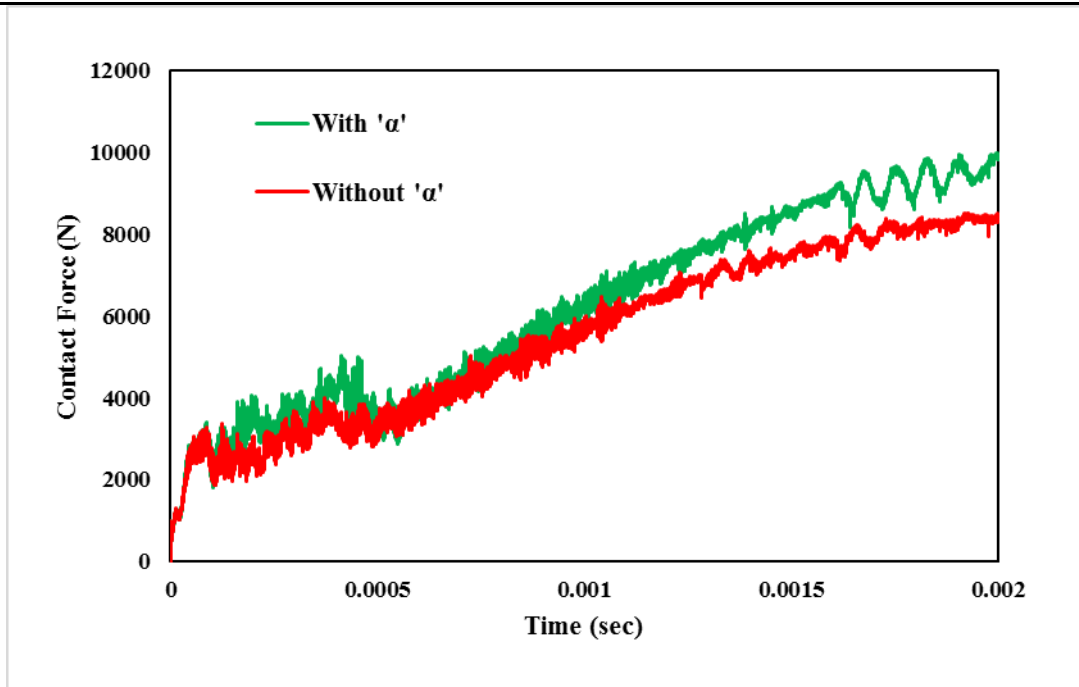


Figure 14: Contact force - time history predicted by the thick plate model on a $[45_{22}]$ E-glass/Epoxy laminate with and without ' α '

5. Conclusions

A micro-mechanics based material model is implemented into an explicit dynamic finite element code LS-DYNA and is used for simulating the behavior of composite structures under impact loading. The model assumes a representative volume cell and the effective stresses of the unit cell are calculated based on the iso-strain boundary conditions between the fiber and resin sub-cells. The non-linear behavior of the resin is accounted with the help of a visco-plastic state variable model proposed by Goldberg [20], [21]. This model represents both the strain-rate dependency and the pressure dependency usually encountered in polymeric materials.

Progressive post-failure behavior is modeled using a CDM based damage model. Different Weibull damage functions are used for various failure modes such as fiber failure, matrix cracking and delamination and the response of the composite is softened depending to the failure mode. The problem of determining the damage/softening exponents in the damage functions has been addressed using a fast-iterative algorithm from within the constitutive model itself. The procedure discussed in this algorithm assigns physical significance to these exponents indirectly and even accounts for the strain localization typically observed in FE models.

All the above discussed characteristics of the micro-mechanics model make it unique and very suitable for impact simulations, validation of which is presented in the current study for impact on E-Glass/Epoxy laminates with different configurations. Contact force–time histories predicted by the model are found to agree very well with experimental results. In addition, the effect of hydrostatic stresses on the peak impact force is studied in detail and the inclusion of this characteristic of the polymer has been observed to aid in predicting more accurate results thereby establishing its significance.

References

- [1] F. Collombet, X. Lalbin, and J. L. Lataillade, "Impact behavior of laminated composites: physical basis for finite element analysis," *Compos. Sci. Technol.*, vol. 58, no. 3–4, pp. 463–478, 1998.
- [2] S. Abrate, "Impact on Laminated Composite Materials," *Appl. Mech. Rev.*, vol. 44, no. 4, pp. 155–190, 1991.
- [3] S. Abrate, "Impact on Laminated Composites: Recent Advances," *Appl. Mech. Rev.*, vol. 47, no. 11, pp. 517–544, 1994.
- [4] K. V. Williams and R. Vaziri, "Application of a damage mechanics model for predicting the impact response of composite materials," *Comput. Struct.*, vol. 79, no. 10, pp. 997–1011, 2001.
- [5] H. M. Hsiao and I. M. Daniel, "Strain rate behavior of composite materials," *Compos. Part B Eng.*, vol. 29, no. 5, pp. 521–533, 1998.
- [6] V. P. W. Shim, C. T. Lim, and K. J. Foo, "Dynamic mechanical properties of fabric armour," *Int. J. Impact Eng.*, vol. 25, no. 1, pp. 1–15, 2001.
- [7] Ö. Akil, U. Yildirim, M. Güden, and I. W. Hall, "Effect of strain rate on the compression behaviour of a woven fabric S2-glass fiber reinforced vinyl ester composite," *Polym. Test.*, vol. 22, no. 8, pp. 883–887, 2003.
- [8] R. K. Goldberg, "Strain Rate Dependent Deformation and Strength Modeling of a Polymer Matrix Composite Utilizing a Micromechanics Approach," 1999.
- [9] A. Gilat, R. K. Goldberg, and G. D. Roberts, "Experimental study of strain-rate-dependent behavior of carbon/epoxy composite," *Compos. Sci. Technol.*, vol. 62, pp. 1469–1476, 2002.
- [10] M. Teratsubo, Y. Tanaka, and S. Saeki, "Measurement of stress and strain during tensile testing of gellan gum gels: Effect of deformation speed," *Carbohydr. Polym.*, vol. 47, no. 1, pp. 1–5, 2002.
- [11] T. E. Tay, H. G. Ang, and V. P. W. Shim, "An empirical strain rate-dependent constitutive relationship for glass-fibre reinforced epoxy and pure epoxy," *Compos. Struct.*, vol. 33, no. 4, pp. 201–210, 1995.
- [12] Z. Li and J. Lambros, "Strain rate effects on the thermomechanical behavior of polymers," *Int. J. Solids Struct.*, vol. 38, pp. 3549–3562, 2001.
- [13] A. S. Wineman and K. R. Rajagopal, *Mechanical response of polymers: an introduction*. Cambridge University Press, 2000.
- [14] J. J. Aklonis and W. J. MacKnight, *Introduction to polymer viscoelasticity*, 2nd ed. New York: Wiley, 1983.
- [15] E. Krempl and C. M. Bordonaro, "A State Variable Model for High Strength Polymers," *Polym. Eng. Sci.*, vol. 35, no. 4, pp. 310–316, Feb. 1995.
- [16] S. V. Thiruppukuzhi and C. T. Sun, "Models for the strain-rate-dependent behavior of polymer composites," *Compos. Sci. Technol.*, vol. 61, no. 1, pp. 1–12, 2001.
- [17] W. A. Spitzig and O. Richmond, "Effect of hydrostatic pressure on the deformation behavior of polyethylene and polycarbonate in tension and in compression," *Polym. Eng. Sci.*, vol. 19, no. 16, pp. 1129–1139, Dec. 1979.
- [18] I. M. (Ian M. Ward and J. Sweeney, *An introduction to the mechanical properties of solid polymers*, 2nd ed. John Wiley & Sons, 2004.
- [19] W. J. Chang and J. Pan, "Effects of yield surface shape and round-off vertex on crack-tip fields for pressure-sensitive materials," *Int. J. Solids Struct.*, vol. 34, no. 25, pp. 3291–3320, 1997.
- [20] R. K. Goldberg, G. D. Roberts, and A. Gilat, "Implementation of an Associative Flow Rule Including Hydrostatic Stress Effects into the High Strain Rate Deformation Analysis of Polymer Matrix Composites," *J. Aerosp. Eng.*, vol. 18, no. 1, pp. 18–27, 2005.
- [21] X. Zheng and W. K. Binienda, "Rate-Dependent Shell Element Composite Material Model Implementation in LS-DYNA," *J. Aerosp. Eng.*, vol. 21, no. 3, pp. 140–151, Jul. 2008.
- [22] J. S. Mayes and A. C. Hansen, "A comparison of multicontinuum theory based failure simulation with experimental results," in *Composites Science and Technology*, vol. 64, no. 3, 2004, pp. 517–527.
- [23] C. A. Weeks and C. T. Sun, "Modeling non-linear rate-dependent behavior in fiber-reinforced composites," *Compos. Sci. Technol.*, vol. 58, no. 3–4, pp. 603–611, Mar. 1998.
- [24] S. V. Thiruppukuzhi and C. T. Sun, "Testing and modeling high strain rate behavior of polymeric composites," *Compos. Part B Eng.*, vol. 29, no. 5, pp. 535–546, 1998.
- [25] A. Matzenmiller, J. Lubliner, and R. L. Taylor, "A constitutive model for anisotropic damage in fiber-composites," *Mech. Mater.*, vol. 20, no. 2, pp. 125–152, 1995.
- [26] C.-F. Yen, "Ballistic impact modelling of composite materials," in *Proceedings of the 7th International LS-DYNA Users Conference*, 2002, pp. 15–26.
- [27] S. Van Hoof, J. Worswick, M.J., Straznicki, P.V., Bolduc, M., Tylko, "Simulation of the Ballistic Impact Response of Composite Helmets," in *5th International LS-DYNA Users Conference, Southfield, Michigan*, 1998.
- [28] A. Tabiei, W. Yi, and R. Goldberg, "Non-linear strain rate dependent micro-mechanical composite material model for finite element impact and crashworthiness simulation," *Int. J. Non. Linear. Mech.*, vol. 40, no. 7, pp. 957–970, 2005.
- [29] A. Tabiei and S. B. Aminjirkarai, "A strain-rate dependent micro-mechanical model with progressive post-failure behavior for

- predicting impact response of unidirectional composite laminates,” *Compos. Struct.*, vol. 88, no. 1, pp. 65–82, 2009.
- [30] R. K. Goldberg, G. D. Roberts, and A. Gilat, “Incorporation of mean stress effects into the micromechanical analysis of the high strain rate response of polymer matrix composites,” *Compos. Part B Eng.*, vol. 34, no. 2, pp. 151–165, 2003.
- [31] D. A. Pecknold and S. Rahman, “Micromechanics-based structural analysis of thick laminated composites,” *Comput. Struct.*, vol. 51, no. 2, pp. 163–179, Apr. 1994.
- [32] A. Tabiei and Q. Chen, “Micromechanics Based Composite Material Model for Crashworthiness Explicit Finite Element Simulation,” *J. Thermoplast. Compos. Mater.*, vol. 14, no. 4, pp. 264–289, 2001.
- [33] S. Medikonda, A. Tabiei, and R. Hamm, “A Comparative study on the Effect of Representative Volume Cell (RVC) Boundary Conditions on the Elastic Properties of a Micromechanics Based Unidirectional Composite Material Model,” *Int. J. Compos. Mater.*, vol. 7, no. 2, pp. 51–71, 2017.
- [34] S. Medikonda and A. Tabiei, “A nonlinear strain rate and pressure-dependent micro-mechanical composite material model for impact problems,” *J. Thermoplast. Compos. Mater.*, p. 89270571774329, 2017.
- [35] J. Qu and M. Cherkaoui, “Effective Properties of Fiber-Reinforced Composite Laminates,” in *Fundamentals of Micromechanics of Solids*, Hoboken, NJ, USA: John Wiley & Sons, Inc., 2006, pp. 214–244.
- [36] A. Tabiei and I. Ivanov, “Micro-mechanical model with strain-rate dependency and damage for impact simulation of woven fabric composites,” *Mech. Adv. Mater. Struct.*, vol. 14, no. 5, pp. 365–377, 2007.
- [37] Z. Bazant and B. Oh, “Crack band theory of concrete,” *Mater. Struct.*, vol. 16, pp. 155–177, 1983.
- [38] S. T. Pinho, L. Iannucci, and P. Robinson, “Physically based failure models and criteria for laminated fibre-reinforced composites with emphasis on fibre kinking. Part II: FE implementation,” *Compos. Part A Appl. Sci. Manuf.*, vol. 37, no. 5, pp. 766–777, 2006.
- [39] O. Cousigné, D. Moncayo, D. Coutellier, P. Camanho, H. Naceur, and S. Hampel, “Development of a new nonlinear numerical material model for woven composite materials accounting for permanent deformation and damage,” *Compos. Struct.*, vol. 106, pp. 601–614, 2013.
- [40] X. Zheng, “Nonlinear Strain Rate Dependent Composite Model for Explicit Finite Element Analysis,” University of Akron, 2006.